Available online at www.sciencedirect.com

ScienceDirect

Procedia CIRP 58 (2017) 251 – 256

www.elsevier.com/locate/procedia

16th CIRP Conference on Modelling of Machining Operations

A coupled Eulerian Lagrangian model to predict fundamental process variables and wear rate on ferrite-pearlite steels

M. Saez-de-Buruaga[a,*], J.A. Esnaola[a], P. Aristimuno[a], D. Soler[a], T. Björk[b], P.J. Arrazola[a]

[a]*Mondragon University, Loramendi kalea 4,20500 Mondragon, Spain*
[b]*Swerea KIMAB AB,Box 7047, 16407 Kista, Sweden*

* Corresponding author. Tel.: +34 943 79 47 00; fax: +34 943 79 15 36. *E-mail address:* msaez@mondragon.edu

Abstract

A coupled Eulerian-Lagrangian Finite Element model of the orthogonal cutting process was developed to predict the influence that ferrite-pearlite steel variants have on fundamental process variables and tool wear. As a case study, this paper is focused on two different ferrite-pearlite inclusion free alloys, where mainly the influence of ferrite-pearlite ratio was tested. Flow stress behavior based on dynamic compression tests and thermal properties function of temperature were characterized for model input parameters. The numerical model is compared with orthogonal cutting tests where the cutting and feed forces, tool temperature, chip morphology and tool wear related variables were measured. Globally, predicted tendencies match with experiments in forces and temperatures. Widest differences on predictions were found for chip thickness and tool-chip contact length. Predicted wear rates are in accordance to experimentally measured values.

Peer-review under responsibility of the scientific committee of The 16th CIRP Conference on Modelling of Machining Operations

Keywords: Finite element method (FEM); Micro structure; Wear

1. Introduction

Tool wear is of great importance in machining processes and has significant impact on process cost and the quality of machined components. Tool wear depends mainly on thermo-mechanical loads and chemical effects generated at the tool chip contact area. These physical effects may become in various types of wear (adhesion, abrasion, diffusion) generating different geometrical wear regions on the tool [1]. Specifically, the wear situated on the rake face (crater wear, KT) and flank wear (VB) are linked to tool life. Therefore, several studies are found in literature on relating material properties with tool wear [2, 3].

The influence that workpiece material has on tool wear has been widely analyzed. Issues such as material composition, heat treatment and the processing method affect physical and thermomechanical properties of materials and their microstructure. These factors in turn affect wear behavior during subsequent processing by machining [2, 3].

The evolution of tool wear related to workpiece material has been tried to be characterized during the last decade. Phenomenological wear rate laws based on experiments or inverse analysis studies taking into account workpiece and tool interface phenomena have been developed [4].

With the aim to reduce the costs of empirical tests to determine machinability, finite element based numerical modelling could become an important tool for wear predictions. In the beginnings of the last decade, previously developed wear rate models such as the ones developed by Usui *et al.* [5] or Takeyama *et al.* [6] started to be implemented in 2D specific purpose codes [7]. These ones were mostly focused on flank wear prediction, simulating the tool wear by nodal displacement. Furtherly, several authors improved the algorithm for crater and flank wear [8]. 3D tool wear models of nose turning have also been published [9] or

Peer-review under responsibility of the scientific committee of The 16th CIRP Conference on Modelling of Machining Operations
doi:10.1016/j.procir.2017.03.194

even coupled tool wear models, where adhesive or diffusive wear models depending on tool temperature could be distinguished [10].

Numerous machining models have been developed in last decades [4]. As mentioned in the previous paragraph, most of the tool wear related modelling is focused on added subroutines in specific purpose codes. These codes are mostly based on lagrangian formulations where the chip formation is obtained by element remeshing or element deletion routines, being a widely-accepted methodology for machining modelling. As alternative to this numerical costly models, authors as Ducobú *et al.* [11] have developed Coupled Eulerian Lagrangian (CEL) models of the chip formation process. These models avoid the need of workpiece remeshing or even element deletion to make possible the chip to be generated.

This paper, sets out a comparison between numerical and experimental framework to validate a CEL technique for modelling machinability effects, focused on ferrite-pearlite steels. In the first step, fundamental variables such as cutting force, feed force, tool temperature, contact length and chip thickness are studied numerically and experimentally.

As a second step, comparison of wear rate between experiments and model is carried out.

Nomenclature

V_s	sliding velocity
σ_n	contact pressure
T	local temperature
S	cutting speed
F	feed
VB	flank wear land (based on ISO3685)
KT	crater ear depth (based on ISO3685)
A_{JC}	elastic limit (Johnson Cook law)
B_{JC}	work hardening modulus (Johnson Cook law)
C_{JC}	strain hardening coefficient (Johnson Cook law)
m	thermal softening coefficient (Johnson Cook law)
n	work hardening coefficient (Johnson Cook law)
A	contact coefficient (Usui wear rate law)
E	activation energy (75.35 KJ/mol·K) [6]
R	gas constant coefficient (8.314 KJ/mol·K) [6]

2. Material selection and characterization

As a case study, two free alloyed ferritic-pearlitic steels were selected: C45 and C60 grades. The C45 grade was selected as a widely-employed material in metal machining. With the aim of validating the model in a wider material range, C60 grade was selected due to the higher pearlite content. Higher pearlite is well known to increase tool wear, aspect that was wanted to be reflected in numerical and experimental framework [2]. In the Table 1 measured grain size and ferrite-pearlite ratio are shown.

For modelling purposes, thermal and mechanical characterization of the selected steels is necessary [4]. Plastic behavior of the material was characterized based on dynamic compression tests. The resultant regression to Johnson-Cook flow stress law coefficients for the numerical model are given in the Table 2. Specific heat, conductivity, thermal expansion and density were characterized in function of temperature, detailed in Table 2. Contact and tool material properties were taken from literature [12].

Table 1. Microstructure properties of C45 and C60 steel grades.

	%F	%P	Grain size F	Grain size P
C45	36	64	22-27	22-27
C60	22	78	22-31	31

3. Coupled Eulerian Lagrangian FE Model

An orthogonal cutting Coupled Eulerian Lagrangian (CEL) model was developed under Abaqus 6.14/Explicit platform. The model was composed by two parts: tool and workpiece. The tool was discretized under a lagrangian frame. A lagrangian domain implies that material deformation is linked to a mesh deformation. For the case of the workpiece, an eulerian domain was selected. In this case, the mesh is static and the material flows through the elements while is being deformed.

The eulerian region was divided into two sections. One of them was composed by “filled” elements, modelling the workpiece, and the other was set with “void” elements. Once the chip is generated, the material flows filling the void elements based on a Eulerian Volume Fraction (EVF) without mesh deformation. This EVF represents the ratio of material fraction that the element has, ranging values between 0-1 for totally void or filled elements [13].

As CEL model in Abaqus is only available for 3D cases, taking as an example the work developed by [11], the workpiece was modelled with one element width, trying to make it as closer as possible to a plane strain 2D model. The eulerian region was meshed with 4 µm elements of 10 µm width. As shown in Fig. 1, the workpiece was fixed on the bottom nodes. To ensure that material could not flow outside the eulerian boundary, symmetry constrain was set to the out of plane walls.

The tool was defined as a lagrangian component. The boundary of the tool was taken as a kinematic constraint in the eulerian calculation and the stress from the eulerian cell was used to calculate the resulting surface stress [13]. The tool was modelled with 6 elements width and wider than the workpiece, in order to ensure eulerian material not to flow outside the corners of the tool. The element size on the tool edge was set to 2 µm and 4 µm in the contact faces of the rake and flank faces. The relative movement of the cutting speed was set to the tool as a kinematic constraint.

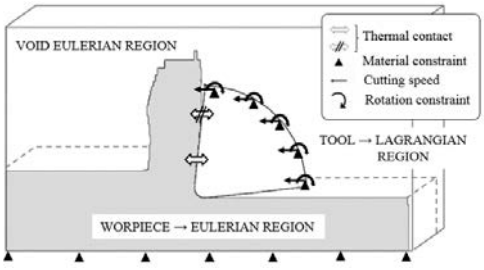

Fig.1. Coupled Eulerian Lagrangian (CEL) model.

Table 2. Input parameters for the FE models.

	Parameters		C45	C60	
Material properties	Johnson Cook parameters	A_{JC} [MPa]	546	570.6	
		B_{JC} [MPa]	452.2	508.7	
		n	0.3514	0.3833	
		C_{JC}	0.0308	0.0378	
		m	0.6146	0.5825	
	Inelastic heat fraction (β)		0.9		
	Density (ρ) [Kg·m^{-3}]		7764	7828	(293 K)
			7684	7747	(573 K)
			7569	7635	(873 K)
	Young modulus [MPa]		$210 \cdot 10^3$		
	Poisson coefficient (ν)		0.3		
	Conductivity (λ) [W·m^{-1}·K^{-1}]		36.1	30.1	(273 K)
			34.3	28.8	(573 K)
			23.2	18.9	(873 K)
	Specific heat (c) [J·Kg^{-1}·K^{-1}]		395.8	430	(273 K)
			545.1	530.8	(573 K)
			632.6	596.6	(873 K)
	Thermal expansion coef.		$6.62 \cdot 10^{-6}$	$4.1 \cdot 10^{-6}$	(293 K)
			$12.5 \cdot 10^{-6}$	$12.6 \cdot 10^{-6}$	(573 K)
			$14.8 \cdot 10^{-6}$	$14.4 \cdot 10^{-6}$	(873 K)
Contact prop.	Thermal cond. [W·m-^{2}·K^{-1}]		10^8		
	Heat transfer coefficient (Γ)		0.5		
	Friction (μ)		0.9		
	% heat friction energy (η)		100		
Tool parameters	Cutting edge radius (rh) [μm]		40		
	Rake angle [º]		6		
	Relieve angle [º]		6		
	Density (ρ) [Kg·m^{-3}]		10600		
	Young modulus [MPa]		$520 \cdot 10^3$		
	Poisson coefficient (ν)		0.22		
	Conductivity (λ) [W·m^{-1}·K^{-1}]		25 (293K)		
	Specific heat (c) [J·Kg^{-1}·K^{-1}]		200 (293K)		
	Thermal expansion coef.		$7.2 \cdot 10^{-6}$ (673K)		
Cutting speed [m·min^{-1}]			100-200		
Feed [mm·rev^{-1}]			0.1-0.2		

Between tool and workpiece the friction was governed by Coulomb friction model limited to the maximum shear stress described in Eq. 1.

$$\tau_f = \mu \cdot \sigma_n \quad \approx \quad \tau_{f\,MAX} = \sigma_{eq} / \sqrt{3} \tag{1}$$

Thermal conductance was set to the model as thermal boundary conditions. A gap conductance of 10^8 W/m^2 was imposed to the contacting pairs when the distance between them was lower than 10^{-7} m. The workpiece and tool temperatures were initially set to room temperature (293 K).

The input parameters for the FE models and the cutting conditions are presented in the Table 2.

4. Orthogonal and tool wear cutting tests

Experimental tests in orthogonal conditions were carried out for model validation (fundamental variables) and characterization of wear rate (wear tests).

For fundamental variable measurement, the employed set-up was detailed in previous publications [14]. This was mounted on a CNC vertical milling machine as shown on Fig. 2. The tool and tool holder were clamped on a dynamometer (Kistler 9121) to measure cutting and feed forces. These and the infrared (IR) camera (FLIR Titanium 550M) were fixed on the moving table of the machine-tool. The orthogonal cutting specimen in form of tube was held on the spindle, giving the rotation movement and the vertical feed. A ground surface was machined on the insert to generate a perpendicular surface for IR measurements, making possible to capture the thermal field on a side view of the tool. As described in [15], experimental thermal measurements were interpolated from the acquiring surface (grinded surface on the tool side) to the mid plane of the tool-chip contact section. The depth of cut of the orthogonal tubes was 2 mm.

For the case of tool wear tests, orthogonal cutting over slotted bars were carried out on a CNC lathe, similar to the work developed by [16]. This approach was selected to reduce the amount of material needed for the essays in comparison to the ones in the milling machine. Tool wear measurements (e.i. crater wear KT, and flank wear VB) were stablished with a confocal profilometer (Alicona Infinite Focus G4)

Tests were developed in four different cutting conditions (cutting speed of 100-200 m/min, and feed of 0.1-0.2 mm). Chips were also collected to validate chip morphology.

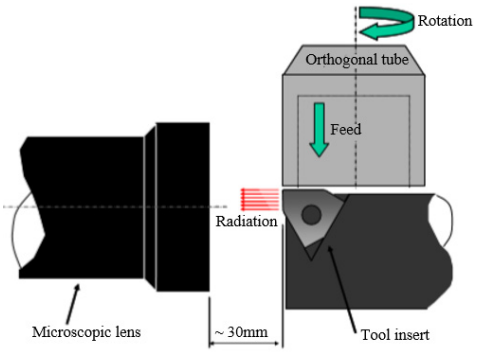

Fig. 2. Developed orthogonal cutting set-up for cutting forces and temperature infrared measurements.

5. Results and discussion

Fundamental variables such as cutting and feed forces, tool temperature, chip thickness and chip-tool contact length were analyzed. As a predictive performance model development, in a second stage tool wear ratios for machinability prediction are compared.

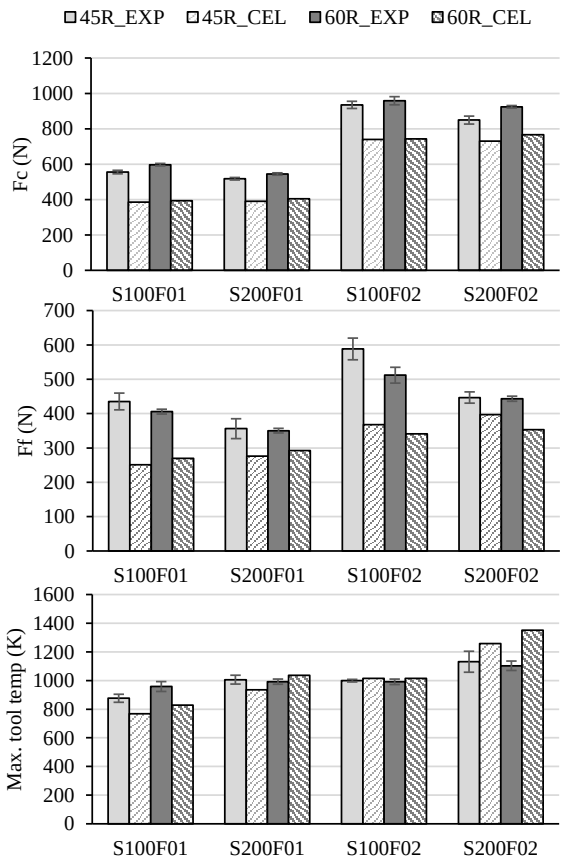

Fig. 3. Comparison of FEM and experimental results of fundamental variables for C45 and C60 grades at 100-200 m/min and 0.1-0.2 mm.

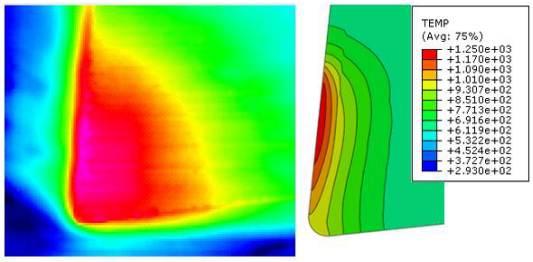

Fig. 4. Thermal field comparison of C45 grade at 200 m/min and 0.2 mm in the mid-plane of the tool-chip contact region.

5.1. Fundamental variables

In the Fig. 3 the fundamental variables comparison between experimental and numerical results are presented.

Focusing on the effect of material selection, the model was sensitive to capture the slight increases on the cutting forces when machining the C60 variant over the C45. In addition, it was also able to capture the decrease on the feed forces at the feed of 0.2 mm between materials.

Globally, the increase on forces due to the increase of the feed was predicted. In turn, the lowering of resultant forces due to the increase of cutting speed was not satisfactory at all. Overall predicted absolute values presented a force underestimation for all the studied cases. This fact was more noticeable for the case of 0.1 mm feed.

In detail, at the feed of 0.2 mm the difference between predictions and experiments was 14% for the cutting forces. Instead, the maximum difference was found to be a 30% in the case of 0.1 mm feed. Analyzing the feed forces, large differences were found again on the case of low feeds. The variations range between 14-42%.

As described, the biggest differences between numerical and experimental forces were found at lower feed conditions. Considering that tool edge radius is 0.04 mm, the ratio between feed and cutting edge radius becomes closer. Consequently, ploughing effect is increased. Thereby, friction behavior in the near tool edge could not be well represented.

In addition, as shown in Fig. 6, the prediction of chip thickness was under estimated, being a direct consequence for the lower cutting forces.

Focusing on temperature measurements, a comparison example of thermal field for the tool-chip contact region is presented in the Fig. 4. Experimentally recorded temperatures on the side view of the tool were interpolated to the mid-plane of the chip contact region [15]. In both cases, experimental and numerical, the maximum temperature is focused on the rake face. Same trend has been obtained for the studied cutting conditions.

Globally, the variations on temperature with the cutting conditions was well reflected in the FE model. The predictions matched nearly without differences at high feed and cutting speeds. The dispersion on the results was greater at a feed of 0.1 mm, achieving there the maximum error of 21%.

Above all, temperature differences at low feeds could be linked also to friction behavior modelled in the near tool edge.

Regarding chip morphology, chip thicknesses were measured by optical microscopy. An example is shown on Fig.5. The Fig. 6 presents the comparison of chip thicknesses and contact lengths.

Globally, the predicted tendencies of contact length, and the longer values of C45 over C60 were in line with the experiments. Negatively, the model estimated lower values than the experimental. Higher differences were found on 0.2 mm conditions, achieving a maximum inaccuracy of a 30%.

A possible explanation for the compared results could be that, during cutting operations, the chip has an oscillation that makes a continuous variation on contact length. For that reason, experimentally measured values correspond to the maximum contact happened, which is eventually longer than the one measured in the numerical model.

In terms of chip thickness, although similar tendencies were predicted, absolute results did not match with the experiments. Numerical model presented a maximum error of 40% at S100F02, while the minimum difference of 18% was set at S200F02. Chip compression ratio on experiments was situated between 2.5-3 in contrast to 1.6-1.9 predicted in the numerical model. Numerically, variations on chip thickness could be linked to the modelled strain hardening behavior of material.

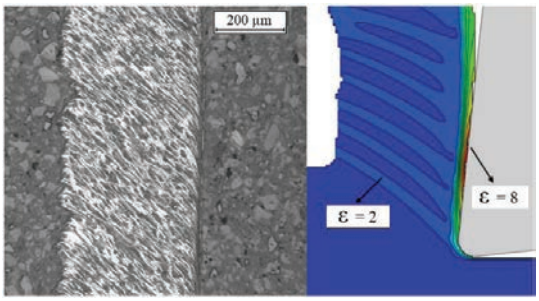

Fig. 5. Chip morphology of C45 grade at 200 m/min and 0.2 mm.

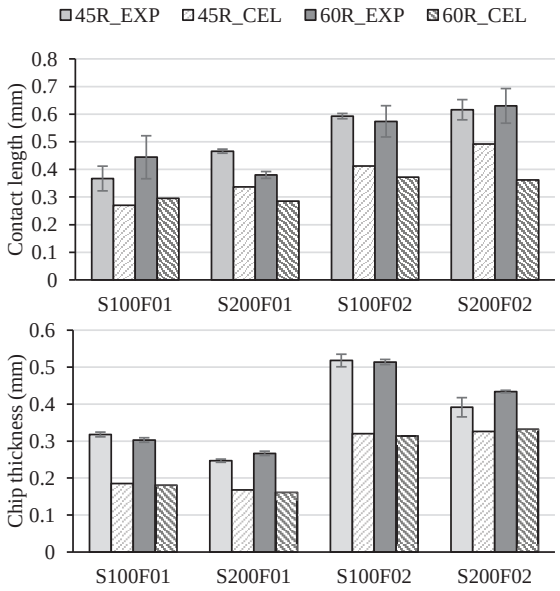

Fig. 6. Comparison of FEM and experimental results of chip thickness and contact length for C45 and C60 grades at 100-200 m/min and 0.1-0.2 mm.

A brief analysis of strain field is presented on Fig. 5. From modelling results, strains on the chip and the primary shear zone obtained values of 1.5-2. For the secondary shear zone, the effect of friction generated strains up to 7-10. Looking to the deformed pearlite grains on the chip, strains of 2-3 were happened, being a closer value with the predicted results.

5.2. Predictive performance: tool wear ratio.

Following the statements supported by [5], wear rate was described as a function of contact pressure, sliding velocity and local temperature. In this case, the thermal activation was set as the activation energy of the diffusion process (E) divided by the universal gas constant (R), being presented first in a wear rate model by [6]. This relationship is presented in Eq. 2.

$$\frac{dW}{dt} = A \cdot \sigma_n \cdot v_s \cdot e^{-E/R \cdot T} \quad (2)$$

Two wear rate regions were compared: crater wear (KT) and flank wear (VB). Fig. 7 shows usual thermal field, sliding velocity and normal pressure distributions along the contact section on the tool. For numerical predictions, wear rate was calculated by taking the medium values of the variables in the specified regions for both, crater and flank wear.

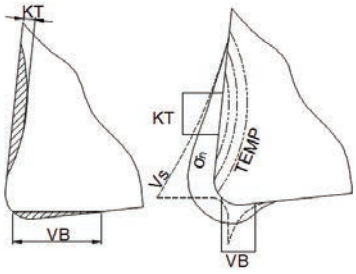

Fig. 7. (a) Wear regions based on ISO3685; (b) wear rate variables.

The evolution of crater wear (KT) and flank wear (VB) was recorded from experimental tests. An example of crater and flank wear evolution is presented in Fig. 8. As cited by [8], wear rate values were extracted in the stable wear region, being there a constant value of the slope. In the Fig. 8 the regression to calculate the wear rate is shown as an example for C60 grade. Wear rate values are compared in Fig. 9 between orthogonal cutting wear experiments and modelling.

To calculate the wear rate on the FE models, the tool-contact parameter was defined based on the minimum square fit between experimental and predicted wear rates in base of an inverse analysis. This parameter was set to be A=1e-10 $m^2 \cdot MN^{-1}$.

Focusing on the main tendencies, modelled flank and crater wear rate matched with the experiments. For both tested grades, the change on wear rate due to the variation on cutting conditions was well achieved. Also, the greatest wear rate found on the C60 over C45 grade was numerically obtained.

Absolute values of wear evolution had some discrepancies between numerical and experimental works. For crater wear rate, at the feed of 0.1 mm the experimental results and predictions matched. At 0.2 mm feed, an underestimation was found when modelling at cutting speed of 100 m/min, and the opposite occurred with 200 m/min, on which the largest differences were found. Analyzing the flank wear evolutions, predicted absolute values lay over the experiments, except at 0.2 mm and 200 m/min where both results came closer.

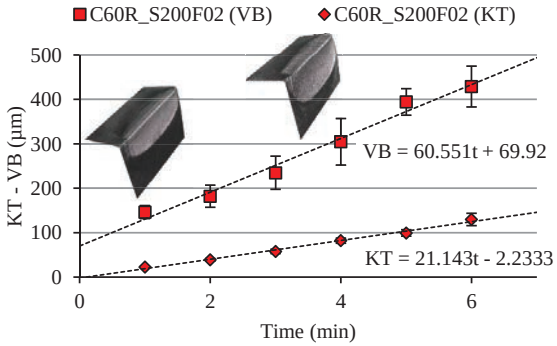

Fig. 8. Example of KT and VB evolution for C60 grade.

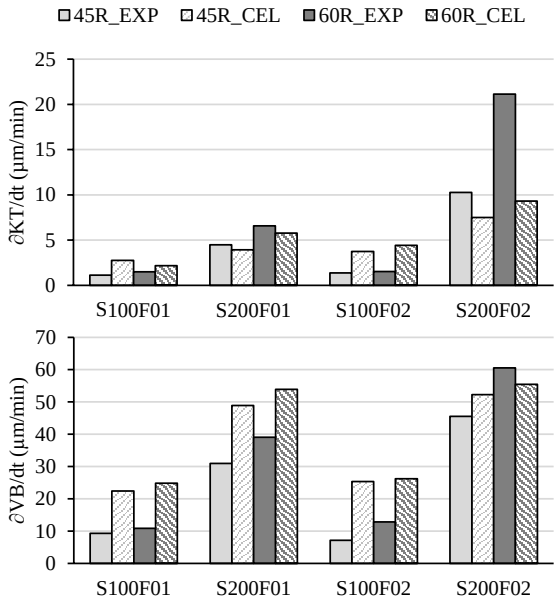

Fig. 9. Comparison of FEM and experimental wear rates for C45 and C60 grades at 100-200 m/min and 0.1-0.2 mm.

In fact, wear rate predictions are in direct relation with fundamental variables. Although the model presented some differences on chip formation, once the contact coefficient of the wear rate law was fitted, procured overall tendencies and absolute wear rate values were in accordance with experiments. But, as concluded previously, an improvement on tool-contact friction behavior and material strain hardening could lead to a better prediction of contact variables, and thus, a better prediction of wear rate evolution.

6. Conclusions

A numerical approach for fundamental variables and wear rate prediction was set with an orthogonal cutting coupled eulerian lagrangian model. For validation, orthogonal cutting tests and wear tests were carried out. Qualitatively, the achieved main conclusions are:

- Predicted cutting and feed force tendencies were comparable to experiments. The decay found on absolute values were more severe in the conditions where the ratio of feed and tool edge radius came closer. The results were affected by the thinner chips simulated.
- Tendencies and absolute values of tool temperature paired with experiments. Only the effect of temperature decrease on C60 over C45 was not well achieved at S200F02.
- Regarding chip thickness and tool-chip contact length, absolute values were under-estimated, although the tendencies seemed to be the same. Friction behavior and modelled material strain hardening could be the main causes for the differences.
- An approach for wear rate prediction was carried out based on Usui [5] wear rate equation. The thermal activation parameter was linked to the diffusive activation energy (E) and the contact parameter (A) was calculated by a regression fitting. Although some differences were found on fundamental variables, identified contact parameter lead to a wear rate prediction that reproduced the experimental tendencies and achieved reasonable absolute values.
- Although it was possible to obtain reasonable wear rate results, care should be paid first to fundamental variable prediction. This could lead to reproduce more realistic contact phenomena, and therefore a better wear rate prediction for all the cutting conditions.

Acknowledgements

The authors thank the projects MICROMAQUINTE (PI_2014_1_116), EMULATE (DP12015-67667-C3-3R) and IMMAC (RFSR-CT-2014-00020) for their funding to the research presented in this paper.

References

[1] Coromant, S. (1994). El mecanizado moderno. Manual Práctico.AB Sandvik Coromant.S-811, 81
[2] Björkeborn, K., Klement, U., & Oskarson, H. (2010). Study of microstructural influences on machinability of case hardening steel. The International Journal of Advanced Manufacturing Technology, 49(5-8), 441-446.
[3] Ozcatalbas, Y., & Ercan, F. (2003). The effects of heat treatment on the machinability of mild steels. Journal of Materials Processing Technology, 136(1), 227-238.
[4] Arrazola, P., Özel, T., Umbrello, D., Davies, M., & Jawahir, I. (2013). Recent advances in modelling of metal machining processes. CIRP Annals-Manufacturing Technology, 62(2), 695-718.
[5] Usui, E., Shirakashi, T., & Kitagawa, T. (1984). Analytical prediction of cutting tool wear. Wear, 100(1), 129-151.
[6] Takeyama, H., & Murata, R. (1963). Basic investigation of tool wear. Journal of Engineering for Industry, 85, 33.
[7] Xie, L., Schmidt, J., Schmidt, C., & Biesinger, F. (2005). 2D FEM estimate of tool wear in turning operation. Wear, 258(10), 1479-1490.
[8] Klocke, F., & Frank, P. (2006). Simulation of tool wear in hard turning. 9th CIRP International Workshop on Modelling of Machining Operations, 11-12.
[9] Attanasio, A., Ceretti, E., Rizzuti, S., Umbrello, D., & Micari, F. (2008). 3D finite element analysis of tool wear in machining. CIRP Annals-Manufacturing Technology, 57(1), 61-64.
[10] Attanasio, A., Ceretti, E., Fiorentino, A., Cappellini, C., & Giardini, C. (2010). Investigation and FEM-based simulation of tool wear in turning operations with uncoated carbide tools. Wear, 269(5), 344-350.
[11] Ducobu, F., Rivière-Lorphèvre, E., & Filippi, E. (2016). Application of the Coupled Eulerian-Lagrangian (CEL) method to the modeling of orthogonal cutting. European Journal of Mechanics-A/Solids, 59, 58-66.
[12] Llanos, I., Villar, J. A., Urresti, I., & Arrazola, P. J. (2009). Finite element modeling of oblique machining using an arbitrary Lagrangian–Eulerian formulation. Machining science and technology, 13(3), 385-406.
[13] Rahulkumar K. Mav (2013), Numerical analysis of bird strike damage on composite sandwich structure using Abaqus/Explicit. San José State University.
[14] Arrazola, P. J., Aristimuno, P., Soler, D., & Childs, T. (2015). Metal cutting experiments and modelling for improved determination of chip/tool contact temperature by infrared thermography. CIRP Annals-Manufacturing Technology, 64(1), 57-60.
[15] Soler, D., Childs, T. H., & Arrazola, P. J. (2015). A note on interpreting tool temperature measurements from thermography. Machining Science and Technology, 19(1), 174-181.
[16] Hosseinkhani, K., & Ng, E. (2015). A combined empirical and numerical approach for tool wear prediction in machining. Procedia CIRP, 31, 304-309.